POLITECNICO DI TORINO
Repository ISTITUZIONALE

Identification of Volterra time-varying parameters in dynamical systems under random excitation

Original
Identification of Volterra time-varying parameters in dynamical systems under random excitation / Scussolini, L., Abbiati, G., Ceravolo, R.. - In: JOURNAL OF SOUND AND VIBRATION. - ISSN 0022-460X. - 645:(2026), pp. 1-18. [10.1016/j.jsv.2026.120128]

Availability:
This version is available at: 11583/3015637 since: 2026-09-16T19:58:34Z

Publisher:
Elsevier

Published
DOI:10.1016/j.jsv.2026.120128

Terms of use:

This article is made available under terms and conditions as specified in the corresponding bibliographic description in the repository

Publisher copyright

(Article begins on next page)

30 October 2026

Journal of Sound and Vibration 645 (2026) 120128

Contents lists available at ScienceDirect

Journal of Sound and Vibration

journal homepage: www.elsevier.com/locate/jsvi

Identification of Volterra time-varying parameters in dynamical systems under random excitation

Linda Scussolini [a,*], Giuseppe Abbiati [b,*], Rosario Ceravolo [a,c]

[a] Department of Structural, Geotechnical and Building Engineering, Politecnico di Torino, Corso Duca degli Abruzzi, 24, Turin, 10129, Italy
[b] Department of Civil and Architectural Engineering, Aarhus Universitet, Inge Lehmanns Gade, 10, C Aarhus, 8000, Denmark
[c] Responsible Risk Resilience interdepartmental Centre (R3C), Politecnico di Torino, Corso Duca degli Abruzzi, 24, Turin, 10129, Italy

ARTICLE INFO

Keywords:
System identification
Non-linear dynamics
Volterra series
Time-frequency domain

ABSTRACT

This paper deals with the estimation of the parameters of non-linear dynamical systems when they are time-varying and the excitation is not measured. This problem is relevant for the structural health monitoring (SHM) field, where input signals are unknown, and system properties can evolve over time due to damage or degradation. In this research, a new identification procedure is proposed, based on the parametrisation of the power spectral density (PSD) of the system response given the PSD of the input. The approach relies on the Volterra series formulation, here extended to time-varying systems, and employs time-frequency transforms that support a running time-domain window interpretation, producing a representation that is causal (i.e., the analysis at any point only uses past/present data, not future data), except for the window's lag. When used for the estimation of time-varying parameters, such transforms lead to an estimation bias that can be related to the analysis window. A benchmark numerical study is conducted on classical Duffing oscillators. Results indicate that the proposed procedure is robust to measurement noise and parameter estimates show negligible bias provided that the Volterra series convergence is satisfied.

1. Introduction

1.1. Background and motivation

The estimation of parameters associated with non-linear systems is a challenging task, especially when these parameters vary over time and the input excitation is unmeasured. This scenario is common in real-world applications, where controlled experiments are impractical, and particularly in the field of structural health monitoring (SHM). Moreover, non-linear responses may arise from different sources, such as geometry, material, damping, or boundary conditions of the system [1]. In such cases, the parameters to be identified are inherently time-varying (e.g., degradation in stiffness and/or strength). An additional well-known challenge in non-linear system identification (SI) consists in unravelling non-linearity from non-stationarity [2], which may not be feasible when the input is not measured.

A common strategy for monitoring systems with time-varying parameters is the instantaneous identification of system features. In the time domain, Bayesian filters can be employed for the identification of instantaneous parameters, including least-squares methods [3], the extended Kalman filter [4], and the unscented Kalman filter [5]. However, time-domain methods lack information on the

* Corresponding authors.
E-mail addresses: linda.scussolini@polito.it (L. Scussolini), abbiati@cae.au.dk (G. Abbiati).

https://doi.org/10.1016/j.jsv.2026.120128
Received 30 September 2025; Received in revised form 7 September 2026; Accepted 10 September 2026
Available online 12 September 2026
0022-460X/© 2026 The Author(s). Published by Elsevier Ltd. This is an open access article under the CC BY license (http://creativecommons.org/licenses/by/4.0/).

frequency components of the signal. In this regard, one may introduce a localisation in time of the signal frequency components [6]. Despite their appeal, most time-frequency methods are not strictly real-time due to the limitations imposed by the time-frequency uncertainty principle [7–9]. Furthermore, the possibility of online implementation depends on the type of transform chosen. Quadratic transforms, particularly those belonging to the Cohen class, offer improved resolution and are invariant under time and frequency shifts, allowing correct physical interpretation [10,11]. However, they are inherently non-causal, as they rely on the correlative structure of the Wigner distribution [12]. In contrast, linear transforms such as the short-time Fourier transform (STFT) decompose the signal into localised components using sliding windows. This structure makes them suitable for causal, and thus potentially real-time, analysis [7].

A key limitation of most time-frequency approaches for SI is the assumption that the input excitation is known. In principle, these approaches could be adapted to the case of unknown input by adopting a Monte Carlo strategy, where multiple input realisations are sampled to infer the system's behaviour statistically. Nevertheless, this may be computationally demanding and often impractical for real-time and/or large-scale applications. A promising alternative arises when the system belongs to a specific subclass of non-linear dynamical systems, characterised by smooth non-linearities (defined here as sufficiently differentiable [13]) and the presence of a stable attractor at the origin. For such systems, it may be possible to estimate the power spectral density (PSD) of the output directly, without requiring knowledge of the input, by using a Volterra series-based approach.

Volterra series extend the concept of Taylor series from functions to functionals by introducing the Volterra kernel, which reflects the higher-order transfer function (TF) of the system. The Volterra theory was extensively developed in the 20th century for the theoretical analysis and kernel estimation of stochastic processes [14,15]. Although several authors proposed methods for estimating higher-order spectra during the second half of the last century, often without explicitly relying on Volterra theory [16,17], it was the work of Lee and Schetzen [18] that provided a concrete and experimentally tractable framework for identifying the non-linear characteristics of a system. Their approach was grounded in the Wiener series representation, which can be interpreted as an orthogonal reformulation of the Volterra series under the assumption of Gaussian white noise excitation. Specifically, the Wiener kernels emerge from a statistical orthogonalisation of the Volterra kernels, allowing each component to be estimated independently. The main reason for the popularity of the approach proposed by Lee and Schetzen is that the leading Wiener kernels can be directly measured via the cross-correlation method, which computes the time-averaged cross-correlations between the system output and products of time-shifted input signals. The Wiener-Lee-Schetzen algorithm led to several developments of cross-correlation techniques for non-linear SI, which can be found in [13,19–23]. However, all these methods suffered from the restrictions given by the model definition, which had to be mainly block-structured (e.g., Wiener, Hammerstein, Uryson) [15]. As a result, the computation of higher-order frequency response function (FRF) was later extended to non-linear autoregressive moving average with exogenous input (NARMAX) models in a more general way [24,25]. Other methodologies employed the harmonic probing method [26] and an explicit definition of cross-cumulants for second- and third-order Volterra systems [27,28].

Volterra-based approaches were then introduced within the SHM community [29–33]. In the context of SI of time-varying non-linear dynamical systems, time-domain methods have been exploited to instantaneously identify non-linear parameters of dynamical systems. Luo and Billings [34] proposed a recursive orthogonal decomposition method based on a rectangular sliding window, capable of adaptively identifying the model structure and parameters online with good numerical stability and limited memory usage, particularly suited for slowly time-varying systems. Another approach, proposed by Weng and Barner [35], considers time-varying Volterra SI within a state-space framework, where variations in the kernel are modelled stochastically and estimated through a Kalman filtering-based method. More recently, a stochastic approach where the Volterra model represents parameters as random variables and uses the maximum entropy principle has been proposed by Villani et al. [36].

However, the development of procedures exploiting Volterra series in a joint time-frequency domain for non-linear SI has been proposed only in a limited number of studies. In particular, Demarie et al. [37] employed the STFT combined with a truncated Volterra series to perform time-frequency identification of weakly non-linear systems, extracting instantaneous modal properties and non-linearities. The STFT combined with a Volterra approach can also be found in Ceravolo et al. [38], modelling the non-linear restoring force through time-varying polynomial coefficients derived from the Volterra kernels with the aim of identifying a degrading hysteretic behaviour over time. Gkikas [39] used the Hilbert-Huang transform combined with the Volterra-Wiener theory by expressing the non-linear system through Wiener-Hammerstein cascades whose polynomial coefficients and impulse responses are identified in a time-frequency framework. Across these studies, some major challenges arise when performing instantaneous parameter estimation: (i) reducing the computational burden associated with the instantaneous estimation of Volterra-based models; (ii) dealing with the case of an input excitation which is not directly measurable; (iii) mitigating the distortions introduced by time-frequency windowing.

1.2. Scope

In this work, starting from [29,40], an instantaneous estimator for joint input-parameter estimation of non-linear dynamical systems is developed. More specifically, Volterra theory is employed to model the instantaneous PSD of the response of non-linear systems subject to random excitation. The underlying model structure is assumed to be known a priori, and the associated parameters are estimated from the measured signals, focusing on parameter estimation rather than detection and localisation. The main contribution of this work is the identification of the system's parameters in the case where the input is not directly measurable but can be described by a parametrisable PSD. The proposed method is specifically designed for white noise excitation, as for this case an analytical expression of the PSD is available from Volterra theory. A key aspect of the proposed approach is the explicit consideration of distortions introduced by windowing in time-frequency transforms. In particular, the estimator compensates for these effects by convolving the

response spectrum with the spectrum of the window. The effectiveness of the proposed estimator is demonstrated using a numerical benchmark study on a classical Duffing oscillator. The paper is organised as follows. Section 2 describes the methodology employed in this paper, including the numerical implementation of the parameter estimation algorithm. Section 3 introduces the case study, while Section 4 validates the proposed procedure in the time-invariant case. In Section 5, a benchmarking of the time-frequency estimator on the same system with time-varying characteristics is carried out. Section 6 proposes an example of application on a 2-degree-of-freedom (DoF) chain-like system under simulated laboratory conditions. Finally, conclusions are drawn in Section 7.

2. Methodology

2.1. Volterra series

For a generic non-linear dynamical system associated with a single attractor at the zero state and a differentiable, smooth non-linearity, the Volterra series expresses the time-domain response in the following form[1]:

$$y(t) \approx \sum_{p=0}^{m} y^{(p)}(t) \tag{1}$$

where $y^{(0)}$ is a constant, and the components $y^{(1)}, \dots, y^{(m)}$ are defined as:

$$y^{(1)}(t) = \int_{-\infty}^{+\infty} h^{(1)}(\tau_1) u(t-\tau_1) \mathrm{d}\tau_1 \tag{2}$$

$$y^{(2)}(t) = \int_{-\infty}^{+\infty} \int_{-\infty}^{+\infty} h^{(2)}(\tau_1, \tau_2) u(t-\tau_1) u(t-\tau_2) \mathrm{d}\tau_1 \mathrm{d}\tau_2 \tag{3}$$

$$\vdots$$

$$y^{(m)}(t) = \int_{-\infty}^{+\infty} \cdots \int_{-\infty}^{+\infty} h^{(m)}(\tau_1, \dots, \tau_m) u(t-\tau_1) \dots u(t-\tau_m) \mathrm{d}\tau_1 \dots \mathrm{d}\tau_m \tag{4}$$

where m is the chosen truncation order of the series, $y^{(p)}(t)$ the p-th component of the response of the system, $h^{(m)}(\tau_1, \dots, \tau_m)$ the m-th order Volterra kernel, and $u(t)$ the system excitation. For the sake of simplicity, and without loss of generality, it is assumed $y^{(0)} = 0$. For the formulation of the case $y^{(0)} \neq 0$, one may refer to [41]. Notably, $h^{(m)}(\tau_1, \dots, \tau_m)$ is symmetric with respect to the sorting of the input arguments[2], and generalises the concept of the linear impulse response function (IRF) to account for higher-order interactions in the system. It follows that truncation of the Volterra series at the first-order provides an exact representation for linear systems. The m-th order Volterra kernel transform $H^{(m)}(\omega_1, \dots, \omega_m)$, here referred to as generalised frequency response function (GFRF), is defined as:

$$H^{(m)}(\omega_1, \dots, \omega_m) = \int_{-\infty}^{+\infty} \dots \int_{-\infty}^{+\infty} h^{(m)}(\tau_1, \dots, \tau_m) e^{-\mathrm{i}(\omega_1 \tau_1 + \dots + \omega_m \tau_m)} d\tau_1 \dots d\tau_m \tag{5}$$

By Fourier transforming[3] Eq. (4), and exploiting the kernel definition of Eq. (5), one has:

$$\begin{aligned} Y^{(m)}(\omega) = \frac{1}{(2\pi)^m} \int_{-\infty}^{+\infty} \dots \int_{-\infty}^{+\infty} \delta(\omega - \omega_1 - \dots - \omega_m) H^{(m)}(\omega_1, \dots, \omega_m) \\ \times U(\omega_1) \dots U(\omega_m) d\omega_1 \dots d\omega_m \end{aligned} \tag{6}$$

with $\delta(\omega - \omega_1 - \dots - \omega_m)$ as the Dirac delta function and $U(\omega)$ as the Fourier transform of the input excitation $u(t)$. Eq. (6) can further be simplified to:

$$\begin{aligned} Y^{(m)}(\omega) = \frac{1}{(2\pi)^{m-1}} \int_{-\infty}^{+\infty} \dots \int_{-\infty}^{+\infty} H^{(m)}(\omega_1, \dots, \omega_{m-1}, \omega - \dots - \omega_{m-1}) \\ \times U(\omega_1) \dots U(\omega_{m-1}) U(\omega - \dots - \omega_{m-1}) \, d\omega_1 \dots d\omega_{m-1} \end{aligned} \tag{7}$$

Consequently, Eq. (1) can be written in the frequency domain as:

$$Y(\omega) \approx \sum_{p=1}^{m} Y^{(p)}(\omega) \tag{8}$$

[1] In its infinite, convergent form, the series provides an exact representation of the system output. However in any practical scenario, the series is truncated resulting in an approximation.

[2] For $m = 2$, the symmetry entails that $h^{(2)}(\tau_1, \tau_2) = h^{(2)}(\tau_2, \tau_1)$.

[3] The definition of the Fourier transform of a generic signal $y(t)$ is here intended as $Y(\omega) = \mathcal{F}\{y(t)\} = \int_{-\infty}^{+\infty} y(t) e^{-\mathrm{i}\omega t} dt$.

When the input is a Gaussian white noise of PSD[4] S_{uu}, the even terms disappear, and the cross input-output PSD S_{yu} is given by the following expression:

$$S_{yu}(\omega) = \Lambda(\omega) S_{uu}(\omega) = \sum_{p=1}^{\frac{m+1}{2}} S_{y^{(2p-1)}u}(\omega) \tag{9}$$

where:

$$\begin{aligned} S_{y^{(2p-1)}u}(\omega) = \frac{(2p)! S_{uu}(\omega)}{p! 2^p (2\pi)^{p-1}} \int_{-\infty}^{+\infty} \dots \int_{-\infty}^{+\infty} H^{(2p-1)}(\omega_1, -\omega_1, \dots, \omega_{p-1}, -\omega_{p-1}, \omega) \\ \times S_{uu}(\omega_1) \dots S_{uu}(\omega_{p-1}) d\omega_1 \dots d\omega_{p-1} \end{aligned} \tag{10}$$

and the index $2p-1$ is used to enforce the selection of odd terms only as explained in [29]. Similarly, the *composite* FRF $\Lambda(\omega)$, reported in Eq. (9), can be calculated directly exploiting the Volterra series approach as:

$$\begin{aligned} \Lambda(\omega) = \sum_{p=1}^{\frac{m+1}{2}} \frac{(2p)!}{p!\, 2^p\, (2\pi)^{p-1}} \int_{-\infty}^{+\infty} \dots \int_{-\infty}^{+\infty} H^{(2p-1)}(\omega_1, -\omega_1, \dots, \omega_{p-1}, -\omega_{p-1}, \omega) \\ \times S_{uu}(\omega_1) \dots S_{uu}(\omega_{p-1}) d\omega_1 \dots d\omega_{p-1} \end{aligned} \tag{11}$$

If one considers the case of a white noise input with constant PSD, that is, $S_{uu}(\omega) = P$, Eq. (10) becomes:

$$S_{y^{(2p-1)}u}(\omega) = \frac{(2p)! P^p}{p! 2^p (2\pi)^{p-1}} \int_{-\infty}^{+\infty} \dots \int_{-\infty}^{+\infty} H^{(2p-1)}(\omega_1, -\omega_1, \dots, \omega_{p-1}, -\omega_{p-1}, \omega) d\omega_1 \dots d\omega_{p-1} \tag{12}$$

Thus, the composite FRF in the case of white noise $\Lambda(\omega)$ can be written as:

$$\Lambda(\omega) = \sum_{p=1}^{\frac{m+1}{2}} \frac{(2p)! P^{p-1}}{p!\, 2^p\, (2\pi)^{p-1}} \int_{-\infty}^{+\infty} \dots \int_{-\infty}^{+\infty} H^{(2p-1)}(\omega_1, -\omega_1, \dots, \omega_{p-1}, -\omega_{p-1}, \omega) d\omega_1 \dots d\omega_{p-1} \tag{13}$$

This analytical expression of the composite FRF is particularly convenient for time-frequency analysis. Indeed, by properly accounting for the windowing function [42], it allows the tracking of the system's frequency components over time, making it suitable for time-frequency SI approaches.

2.2. Time-frequency estimator

In the resolution of the inverse problem, the basic idea of time-frequency approaches is to exploit bi-dimensional (joint) functions $\tilde{\mathbf{T}}_y(t, \omega)$, referred to as time-frequency representations of the generic signal $y(t)$, to find a model that produces the same distribution of a given measured signal. In general, this can be achieved by minimising the distance between the time-frequency model $\mathbf{T}_y(t, \omega; \mathbf{p})$ and the time-frequency transform of the measured signal $\tilde{\mathbf{T}}_y(t, \omega)$. The time-frequency model is defined in terms of the global vector of parameters $\mathbf{p} = \{p_1, p_2, \dots, p_k, \dots, p_{K-1}, p_K\}$, with p_k as the k-th parameter to be estimated and K as the total number of parameters.

In time-frequency analysis *instantaneous* quantities refer to a specific point in time whereas *local* quantities must be intended as estimates of *instantaneous* quantities obtained on windowed data [43]. The proposed framework provides a *local* estimator $\mathbf{p}_{\text{opt}}$ for the *instantaneous* value of the parameter vector $\mathbf{p}$, which is obtained by solving the following optimisation problem:

$$\mathbf{p}_{\text{opt}}(\bar{t}) = \arg\min_{\mathbf{p}} J(\bar{t}, \mathbf{p}) \tag{14}$$

where the cost function $J(\bar{t}, \mathbf{p})$ is computed for a running window localised at $\bar{t}$ as:

$$J(\bar{t}, \mathbf{p}) = \| \mathbf{T}_{y_\gamma}(\bar{t}, \omega; \mathbf{p}) - \tilde{\mathbf{T}}_{y_\gamma}(\bar{t}, \omega) \|^2_{2, \mathcal{D}_\omega} \tag{15}$$

with $\omega \in \mathcal{D}_\omega$. In this work, the predicted time-frequency spectrum $\mathbf{T}_{y_\gamma}(\bar{t}, \omega; \mathbf{p})$ is computed using a Volterra series representation under white noise excitation. Thus, one may exploit the formulation of the PSD reported in Eq. (10) as the time-frequency transform. In particular, the analytical form of the Volterra kernel is known from the non-linear model (e.g., the generic polynomial representation), and only the parameters entering these analytical expressions are estimated from the measured data. Similarly, since the excitation is white noise, the input spectrum S_{uu} corresponding to the variance P is also estimated. Although here the time-frequency transform refers to a single input-output systems, the formulation is general and can be extended to systems with multiple inputs and/or outputs.

Introducing γ as a short-time analysis window, the resulting model can be expressed by combining cross-spectral estimations over multiple windows γ. This approach allows for an examination of the temporal evolution of frequency components shared between the signals, with each window providing a localised time frame over which the output PSD is estimated. For this purpose, let us again consider a system where the generic signals $y(t)$ and $u(t)$ are the measured output and input. The measured time-frequency transform $\tilde{\mathbf{T}}_{y_\gamma}(t, \omega)$, evaluated at the time instant $\bar{t}$, can be considered the instantaneous PSD of the signal. If the Welch's method is exploited,

[4] For a wide-sense stationary random process, the PSD is defined as the Fourier transform of the autocorrelation function.

the PSD is computed by segmenting the signal $y(t)$ into overlapping windows, computing the periodogram for each window, and then averaging. That said, the instantaneous PSD writes:

$$\tilde{\mathbf{T}}_{y_\gamma}(\bar{t},\omega) := \mathbb{E}[Y_\gamma(\bar{t},\omega)Y_\gamma^*(\bar{t},\omega)] \tag{16}$$

where $Y_\gamma(\bar{t},\omega)$ is the Fourier transform of the time-windowed signal $y_\gamma(\bar{t},t)$, defined as:

$$y_\gamma(\bar{t},t) = y(t)\gamma(t-\bar{t}) \tag{17}$$

with $\gamma(t-\bar{t})$ as the window function and $\bar{t}$ again the time localisation of the window. When the window function spans only few system periods, the bias induced on the instantaneous PSD estimate is not negligible. However, such bias can be compensated leveraging the convolution theorem, considering the PSD of the window function [44]. Accordingly, the following time-frequency *corrected estimator* is proposed:

$$\mathbf{T}_{y_\gamma}(\bar{t},\omega;\mathbf{p}) := \frac{S_{yy}(\bar{t},\omega;\mathbf{p}) * S_{\gamma\gamma}(\bar{t},\omega)}{Z} \approx S_{yy}^{\gamma}(\bar{t},\omega;\mathbf{p}) \tag{18}$$

where Z is a normalisation constant, and:

$$S_{yy}(\bar{t},\omega;\mathbf{p}) = \Lambda(\omega;\mathbf{p})S_{yu}(\bar{t},\omega;\mathbf{p}) \tag{19}$$

with $S_{yu}(\bar{t},\omega;\mathbf{p})$ and $\Lambda(\omega;\mathbf{p})$ as defined in Eqs. (9) and (13). The convolution of Eq. (18) reduces the bias of the PSD estimate caused by the window function γ.

2.3. Numerical implementation

This section illustrates the numerical implementation of the proposed time-frequency estimator for a given time window. Time and frequency axes are discretised as:

$$\begin{aligned} t &= \bar{t} + r\Delta t \\ \omega &= s\Delta\omega \end{aligned} \tag{20}$$

where the time index $r \in [0,\dots,T/\Delta t]$ and the frequency $s \in [-T/(2\Delta t),\dots,T/(2\Delta t)]$ with T as the length of the window function γ and Δt as the sampling period of the signals. Accordingly, the discretised sampled output and window function reads:

$$\begin{aligned} y[r] &= y(\bar{t} - T/2 + r\Delta t) \\ \gamma[r] &= \gamma(r\Delta t) \end{aligned} \tag{21}$$

and the following sampled Volterra kernel and input PSD, respectively:

$$\begin{aligned} H^{(p)}[s_1,\dots,s_p;\mathbf{p}] &= H^{(p)}(s_1\Delta\omega,\dots,s_p\Delta\omega;\mathbf{p}) \\ S_{uu}[s] &= S_{uu}(s\Delta\omega) \end{aligned} \tag{22}$$

The numerical implementation of the cost function in MATLAB is reported in the Algorithm 1. For each time window, the algorithm calculates the Fourier transform of the windowed output signal and estimates its local PSD. This measured time-frequency transform is then compared with the model-based PSD computed following Volterra theory. Finally, the objective function is evaluated by minimising the distance between the theoretical and measured PSD.

Algorithm 1 Numerical implementation of the cost function for a single time window.

for $s \in [-T/(2\Delta t),\dots,T/(2\Delta t)]$ **do**
- $Y^\gamma[s] = \sum_r y[r]\gamma[r]\exp(-\mathrm{i}(s\Delta\omega)(r\Delta t))\Delta t$ ▷ Fourier transform of $y[r]$
- $S_{yy}^\gamma[s] = |Y^\gamma[s]|^2$ ▷ Welch-based local PSD estimate
- $\tilde{\mathbf{T}}_{y_\gamma}[s] := S_{yy}^\gamma[s]$ ▷ Measured time-frequency transform
- $S_{yu}[s;\mathbf{p}] = \sum_{p=1}^{\frac{m+1}{2}} S_{y^{(2p-1)}u}[s;\mathbf{p}]$ ▷ Model of the cross-PSD
- $\Lambda[s;\mathbf{p}] = \sum_{p=1}^{\frac{m+1}{2}} \frac{(2p)!P^{p-1}}{p!2^p(2\pi)^{p-1}} \sum_{s_1,\dots,s_{p-1}} H^{(2p-1)}[s_1,-s_1,\dots,s_{p-1},-s_{p-1},s;\mathbf{p}]\Delta\omega^{p-1}$
- $S_{yy}[s;\mathbf{p}] = \Lambda[s;\mathbf{p}]S_{yu}[s;\mathbf{p}]$ ▷ Model of the output PSD
- $\Gamma[s] = \sum_r \gamma[r]\exp(-\mathrm{i}(s\Delta\omega)(r\Delta t))\Delta t$ ▷ Fourier transform of $\gamma[r]$
- $S_{\gamma\gamma}[s] = |\Gamma[s]|^2$ ▷ Window local PSD estimate
- $\mathbf{T}_{y_\gamma}[s;\mathbf{p}] := \frac{S_{yy}[s;\mathbf{p}]*S_{\gamma\gamma}[s]}{Z}$ ▷ Time-frequency estimator

end for

$J(\mathbf{p}) = \frac{\sum_s(\mathbf{T}_{y_\gamma}[s;\mathbf{p}]-\tilde{\mathbf{T}}_{y_\gamma}[s])^2}{\sum_s \tilde{\mathbf{T}}_{y_\gamma}^2[s]+\varepsilon}$ ▷ Objective function

In the present work, the minimisation of $J(\mathbf{p})$ is conducted using gradient-based optimisation as implemented in the *fmincon* MATLAB function. A normalisation preprocessing step is performed on all parameters such that their values lie within [0, 1] interval

Table 1
Parameter values for the Duffing oscillator.

m_t [kg]	k_1 [N/m]	k_3 [N/m^3]	c [Ns/m]	P [−]
1.00	39.48	1000.0	0.38	{0.002, 0.003, 0.004}

to improve the convergence of the optimisation algorithm. Thus, a starting point between 0.1 and 0.3 was considered in the estimation process. Moreover, a tolerance value ε was added to the denominator of the objective function to avoid numerical stability issues.

3. Description of the case study

The proposed time-frequency estimator is benchmarked numerically. A Duffing oscillator is selected as a reference case study owing to its simplicity and the availability of analytical expressions for GFRFs [29,40]. Polynomial non-linearities are infinitely differentiable, making the system smooth, and thus ensuring the existence of the Volterra series. The equation of motion for a symmetric Duffing oscillator is:

$$m_t \ddot{y} + c\dot{y} + f(y) = u(t) \tag{23}$$

with:

$$f(y) = f_l(y) + f_{nl}(y) = k_1 y + k_3 y^3 \tag{24}$$

where m_t is the mass, c is the viscous damping, k_1 and k_3 are the linear and cubic stiffness terms, and $u(t)$ is Gaussian noise with constant PSD $S_{uu}(\omega) = P$. The values of the parameters of the Duffing oscillator are reported in Table 1. The convergence of the Volterra series has been verified for these parameter values following the procedure outlined in [29].

The first two non-zero GFRFs of the Duffing oscillator of Eq. (23) are:

$$H^{(1)}(\omega) = \frac{1}{k_1 - m_t\omega^2 + \mathrm{i}c\omega} \tag{25}$$

$$H^{(3)}(\omega_1, \omega_2, \omega_3) = -\frac{1}{6} H^{(1)}(\omega_1 + \omega_2 + \omega_3)\left(6k_3 H^{(1)}(\omega_1) H^{(1)}(\omega_2) H^{(1)}(\omega_3)\right) \tag{26}$$

and can be obtained via *harmonic probing* as described in [31]. Both GFRFs are shown in Fig. 1. As can be seen from Fig. 1(a), the linear kernel $H^{(1)}$ does not provide a comprehensive representation of the system dynamics, leading to an underestimation of all the peaks given by the GFRF, clearly observable in Fig. 1(b–d). The linear kernel $H^{(1)}$ identifies the global maxima, corresponding to the fundamental frequency of the underlying linear system. However, the local maxima distributed across the $H^{(3)}$-plane, see Fig. 1(b–d), indicate the presence of other peaks, corresponding to the other combinations of frequencies governing the non-linear response of the system. If the system is described by a polynomial of higher order than 3, then the combinations of frequencies governing the non-linear response will increase accordingly.

In accordance with the definition of the kernels reported in Eqs. (25) and (26), in the case of white Gaussian noise, the response in the frequency domain may be calculated reducing it to the problem of cross-spectra definition. The cross-spectra definition for different types of polynomial systems may be found in [40,45,46]. For a white noise input excitation of PSD:

$$S_{uu}(\omega) = P \tag{27}$$

the cross input-output PSD truncated at the 5-th component reads:

$$S_{yu}(\omega) = S_{y^{(1)}u} + S_{y^{(3)}u} + S_{y^{(5)}u} \tag{28}$$

with, for a symmetric Duffing oscillator:

$$S_{y^{(1)}u} = H^{(1)}(\omega)P \tag{29}$$

$$S_{y^{(3)}u}(\omega) = -\frac{3P^2 k_3 H^{(1)}(\omega)^2}{2ck_1} \tag{30}$$

$$S_{y^{(5)}u}(\omega) = \left(\frac{9P^2 k_3^2 H^{(1)}(\omega)^3}{4c^2 k_1^2} + \frac{9P^2 k_3^2 H^{(1)}(\omega)^2}{4c^2 k_1^3} + \frac{9P^2 k_3^2 H^{(1)}(\omega)^2}{2\pi^2} I(\omega)\right) P \tag{31}$$

with $I(\omega)$ defined as in [40]. Accordingly, the resulting composite FRF expressions for expansion orders 1, 3 and 5 are:

$$\Lambda^{(1)}(\omega) = \frac{S_{y^{(1)}u}(\omega)}{S_{uu}(\omega)} = H^{(1)}(\omega) \tag{32}$$

$$\Lambda^{(3)}(\omega) = \frac{S_{y^{(1)}u}(\omega) + S_{y^{(3)}u}(\omega)}{S_{uu}(\omega)} = \Lambda^{(1)}(\omega) - \frac{3Pk_3 H^{(1)}(\omega)^2}{2ck_1} \tag{33}$$

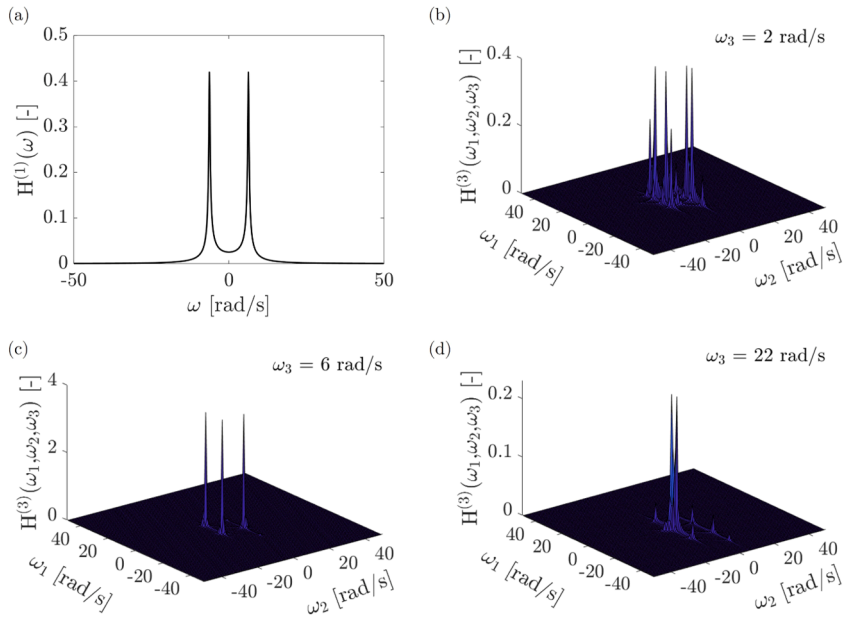


Fig. 1. First-order kernel (a), and third-order kernel at $\omega_3 = 2$, rad/s (b), at $\omega_3 = 6$, rad/s (c), and at $\omega_3 = 22$, rad/s (d).

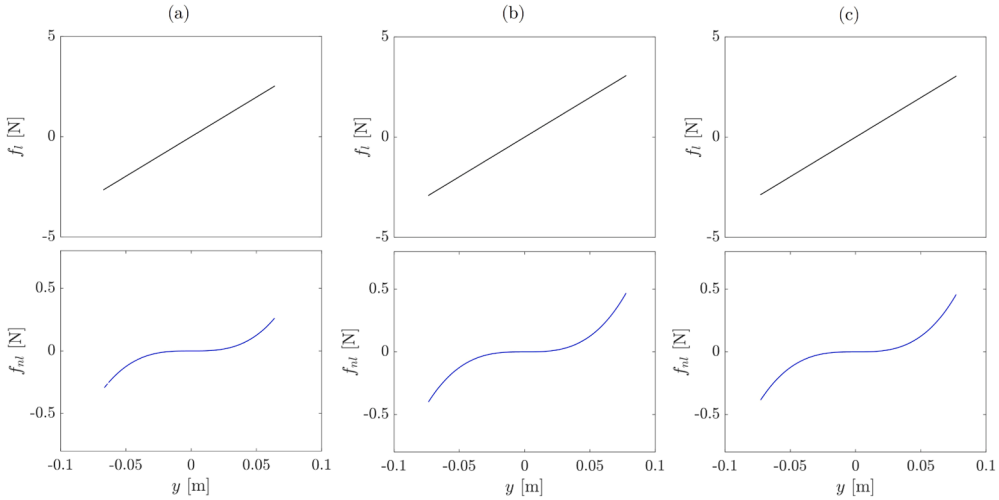


Fig. 2. Linear and non-linear restoring force, f_l and f_{nl}, for $P = 0.002$ (a), $P = 0.003$ (b), and $P = 0.004$ (c).

$$\Lambda^{(5)}(\omega) = \frac{S_{y^{(1)}u}(\omega) + S_{y^{(3)}u}(\omega) + S_{y^{(5)}u}(\omega)}{S_{uu}(\omega)} = \Lambda^{(3)}(\omega) + \frac{9P^2k_3^2H^{(1)}(\omega)^3}{4c^2k_1^2} + \frac{9P^2k_3^2H^{(1)}(\omega)^2}{4c^2k_1^3} + \frac{9P^2k_3^2H^{(1)}(\omega)^2}{2\pi^2}I(\omega) \tag{34}$$

The displacement response of the Duffing oscillator defined in Eq. (23) is computed via numerical integration considering a time step size $\Delta t = 0.005$ s and a simulation span $t_{\max} = 200$ s using the ODE23S MATLAB function[5]. Figs. 2 and 3 show the restoring force and the composite FRF Λ for three cases of variance of the input P. The composite FRF was calculated according to Eqs. (32)–(34). In particular, it is clear how the degree of non-linearity becomes more evident for increasing values of P.

[5] Such function implements the 2nd-order Rosenbrock method.

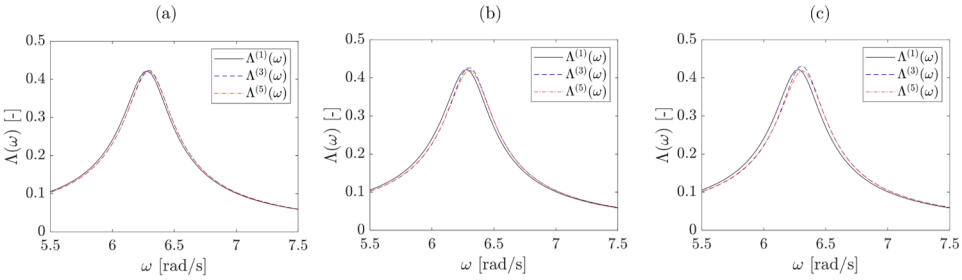


Fig. 3. Composite FRF Λ for $P = 0.002$ (a), $P = 0.003$ (b), and $P = 0.004$ (c).

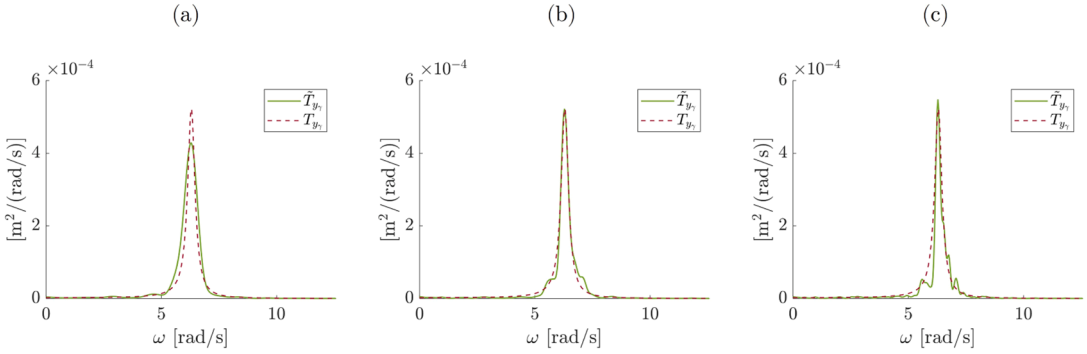


Fig. 4. Corrected estimator vs. measured PSD (expected value computed on 10 segments) for (a) WL = $15T_0$, (b) WL = $30T_0$, and (c) WL = $50T_0$.

4. Validation of the time-frequency estimator

4.1. Validation of the correction factor

The time-frequency estimator is benchmarked to evaluate how accurately the corrected estimator $\mathbf{T}_{y_\gamma}$ approximates the measured PSD $\tilde{\mathbf{T}}_{y_\gamma}$ considering three values for the time window lengths WL:

$$\text{WL} = \{15T_0, 30T_0, 50T_0\} \tag{35}$$

with $T_0 = 2\pi\sqrt{m_t/k_1} = 1$ s as the period of the linearised Duffing oscillator. Fig. 4 compares, for different WL, the corrected estimator $\mathbf{T}_{y_\gamma}$ from Eq. (18) with the measured PSD $\tilde{\mathbf{T}}_{y_\gamma}$ from Eq. (16).

Fig. 4 reveals that the corrected estimator well describes the measured PSD of the system response for all investigated window sizes. As expected, the agreement between the corrected estimator and measured PSD improves for longer WL. However, a residual discrepancy between $\mathbf{T}_{y_\gamma}$ and $\tilde{\mathbf{T}}_{y_\gamma}$ remains, which can be ascribed to i) the uncertainty in the measured PSD $\tilde{\mathbf{T}}_{y_\gamma}(\bar{t}, \omega)$; ii) the bias induced by the windowing function $\gamma(t - \bar{t})$; iii) the truncation of the Volterra series expansion used in the corrected estimator $\mathbf{T}_{y_\gamma}(\bar{t}, \omega; \mathbf{p})$.

4.2. Validation of the estimation procedure

Displacement response signals are contaminated with noise to benchmark the time-frequency estimator. In this study, signal-to-noise ratio (SNR) is defined as [47]:

$$\text{SNR} = \frac{\sigma_y^2}{\sigma_n^2} = \{10.0, 100.0\} \tag{36}$$

where σ_y^2 is the variance of the clean displacement response signal y and σ_n^2 of the added noise. Moreover, the procedure is repeated for different truncation orders m for the Volterra kernel, to prove the results are unbiased with respect to the series convergence. The proposed procedure is benchmarked against a state-of-the-art technique, namely, the augmented unscented Kalman filter (AUKF), implemented as in [48]. The comparison with the AUKF is presented in the time-invariant scenario, since, for rapidly time-varying parameters, such as those considered in this work, the standard AUKF may require prior knowledge of the parameter variations or significant tuning of the process noise covariance to achieve accurate estimates. Similar observations have been reported in [49,50]. In this case, only the linear parameters m_t, c, and k_1 are assumed to be known, while the parameter vector to be estimated is given by $\mathbf{p} = \{k_3, P\}$. The estimation was repeated for 20 realisations of a white-noise input excitation in order to assess the confidence interval of the instantaneous estimator. For each realisation, the system response is numerically integrated using ODE23S in MATLAB. Results are reported in Figs. 5 and 7 for the Volterra series truncation order $m = 3$ and in Figs. 6 and 8 for the Volterra series truncation

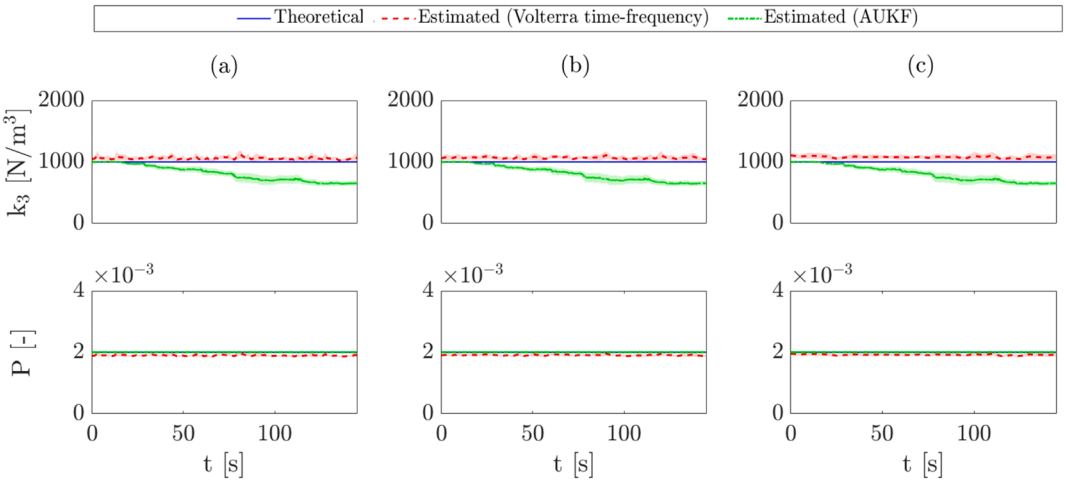


Fig. 5. Joint input-parameter estimation with SNR $= 10$ and $m = 3$ in case of time-invariant k_3 and P: (a) WL $= 15T_0$, (b) WL $= 30T_0$, (c) WL $= 50T_0$.

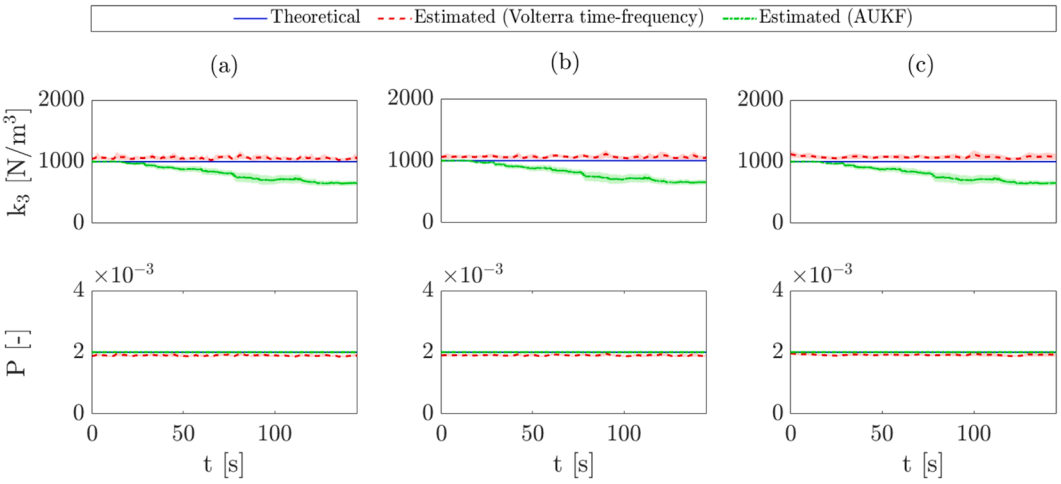


Fig. 6. Joint input-parameter estimation with SNR $= 10$ and $m = 5$ in case of time-invariant k_3 and P: (a) WL $= 15T_0$, (b) WL $= 30T_0$, (c) WL $= 50T_0$.

order $m = 5$; in both cases, the estimation is performed on noise-contaminated response signals for the two levels of SNR reported in Eq. (36), namely, 100 (low noise) and 10 (high noise). The lines correspond to average values while shaded regions represents the 95% confidence bounds for the estimates obtained from 20 realisations. The estimates of k_3 are fairly stable regardless of the noise level in the response data (SNR $= \{10, 100\}$) and the truncation order of the Volterra series ($m = \{3, 5\}$). In both cases, increasing the truncation order of the Volterra series from $m = 3$ to $m = 5$ does not produce any significant change. Therefore, it is concluded that the small bias in the parameter estimates shall be ascribed to the bias induced by the windowing function.

5. Benchmark of the time-frequency estimator (time-varying)

This section presents the results of the numerical benchmarking of the procedure for the estimation of the time-varying parameters of the same Duffing oscillator utilised in Section 4 whose parameters are reported in Table 1. Response data has been synthetically generated considering a SNR $= 100$ and a time span $t_{\max} = 200$ s.

5.1. Parameter estimation

The SI task addressed in this Section is restricted to the estimation of a time-varying cubic stiffness coefficient $k_3(t)$:

$$k_3(t) = 1000 + 500 \sin(0.1t) \tag{37}$$

Therefore, $\mathbf{p} = \{k_3\}$. Fig. 9 shows the estimation results for the parameter k_3 over time, obtained using varying WL. An overlap of 90% was set constant in all the cases. The lines correspond to average values while shaded regions represents the 95% confidence bounds for the estimates obtained from 20 realisations.

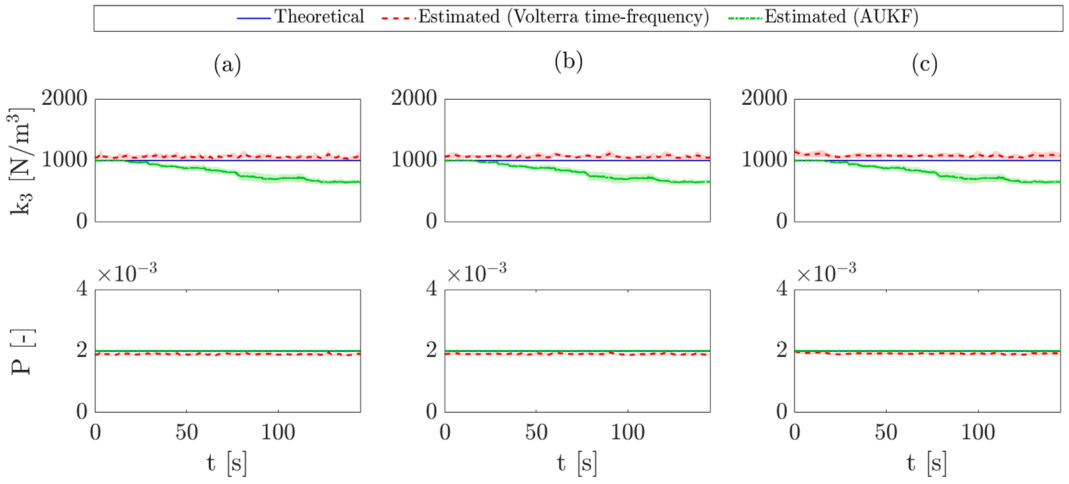


Fig. 7. Joint input-parameter estimation with SNR = 100 and $m = 3$ in case of time-invariant k_3 and P: (a) WL = $15T_0$, (b) WL = $30T_0$, (c) WL = $50T_0$.

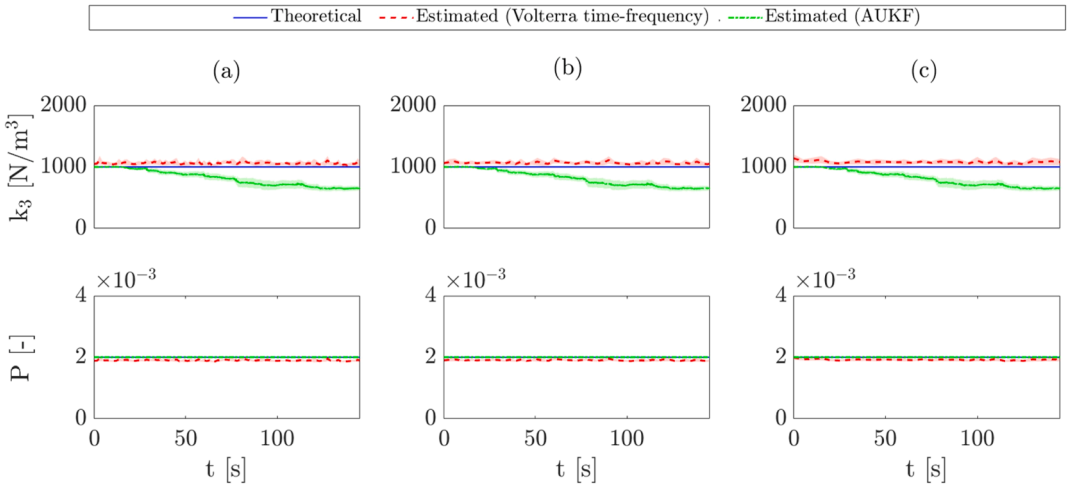


Fig. 8. Joint input-parameter estimation with SNR = 100 and $m = 5$ in case of time-invariant k_3 and P: (a) WL = $15T_0$, (b) WL = $30T_0$, (c) WL = $50T_0$.

As shown in Fig. 9, the proposed estimator captures the variability of $k_3(t)$ for all values of WL and m (i.e., for all realisations results almost coincide). The zoomed view around 45 s shows that the shorter window function WL = $15T_0$ yields an accurate instantaneous estimation of the parameter.

5.2. Input estimation

Here, the SI task involves the estimation of a time-varying input variance $P(t)$:

$$P(t) = \begin{cases} 0.002\ , & 0 \le t < t_1 \\ 0.003\ , & t_1 \le t < t_2 \\ 0.004\ , & t_2 \le t < t_{\text{end}} \end{cases} \tag{38}$$

Therefore, $\mathbf{p} = \{P\}$. Fig. 10 shows the identification results for the parameter P over time, obtained using varying WL. The lines correspond to average values while shaded regions represents the 95% confidence bounds for the estimates obtained from 20 realisations.

As shown in Fig. 10, the proposed estimator accurately tracks the variations of P. As observed also in the case of the non-linear parameter estimation, shorter WL can better capture the variations of P.

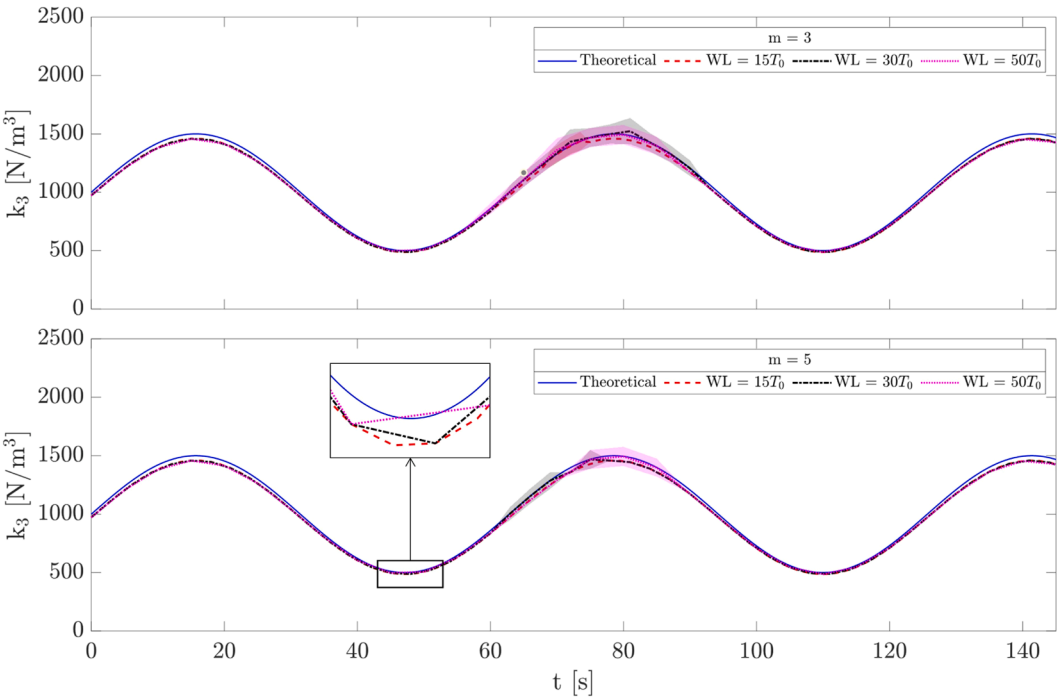


Fig. 9. Estimated time-varying k_3 for several WL as function of the linear period T_0.

5.3. Joint input-parameter estimation

The validation of the framework is carried out for the case of time-varying $k_3(t)$ and $P(t)$, defined according to Eqs. (37) and (38), respectively; therefore, $\mathbf{p} = \{k_3, P\}$. Figs. 11 and 12 illustrate the results of joint input-parameter estimation. The lines correspond to average values while shaded regions represents the 95% confidence bounds for the estimates obtained from 20 realisations.

As shown in Figs. 11 and 12, the proposed estimator successfully tracks both $k_3(t)$ and $P(t)$ with results largely independent of the values of WL and m. This demonstrates the effectiveness of the correction introduced in Eq. (18) in mitigating the bias induced by the analysis window.

5.4. Joint linear and non-linear input-parameter estimation

A common situation in real-world applications is given by the estimation of linear and non-linear parameters simultaneously. Thus, $\mathbf{p} = \{k_1, k_3, P\}$, with k_1 constant and defined according to Table 1. Figs. 13 and 14 illustrate the results of joint input-parameter estimation. The lines correspond to average values while shaded regions represents the 95% confidence bounds for the estimates obtained from 20 realisations.

As can be seen from Figs. 13 and 14, the estimation results both in the case of $m = 3$ and $m = 5$ suggest that including k_1 in the estimation process does not hinder the estimation accuracy of $k_3(t)$ and $P(t)$.

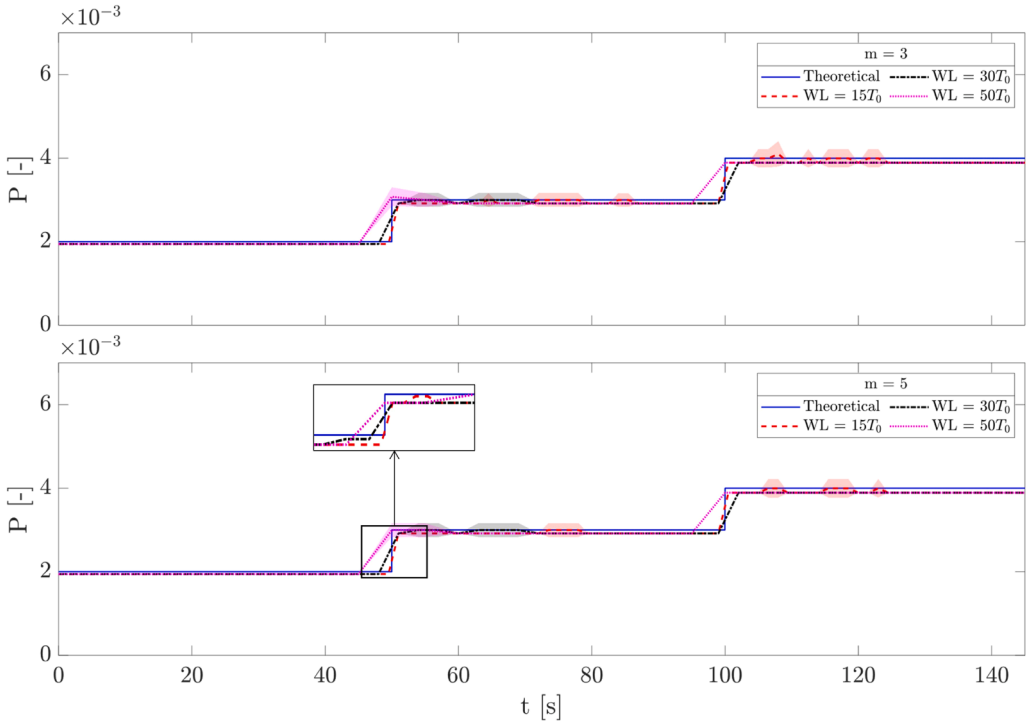


Fig. 10. Estimated time-varying P for several WL as function of the linear period T_0.

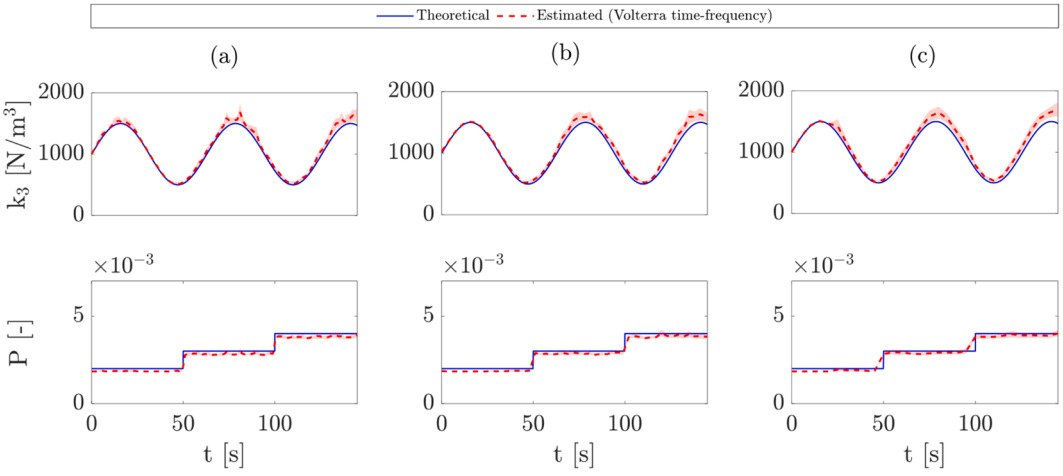


Fig. 11. Joint input-parameter estimation for $m = 3$ in case of time-varying k_3 and P: (a) WL = $15T_0$, (b) WL = $30T_0$, and (c) WL = $50T_0$.

6. Application on a 2-DoF chain-like system

To illustrate the applicability of the proposed methodology beyond the single-DoF Duffing oscillator, a chain-like multi-DoF system is considered, as schematically shown in Fig. 15. Such systems are commonly used as representative models of engineering structures exhibiting non-linear dynamic behaviour, such as frame structures [51].

The system is composed of two equal masses m_t, linked by a linear, quadratic, and cubic stiffness, k_1, k_2, and k_3, respectively. Accordingly, the system dynamics is governed by the following equations:

$$\begin{cases} m_t\ddot{y}_1 + c\dot{y}_1 + k_1(2y_1 - y_2) + k_2(y_1 - y_2)^2 + k_3(y_1 - y_2)^3 = u_1(t) \\ m_t\ddot{y}_2 + c\dot{y}_2 + k_1(2y_2 - y_1) - k_2(y_2 - y_1)^2 + k_3(y_2 - y_1)^3 = u_2(t) \end{cases} \tag{39}$$

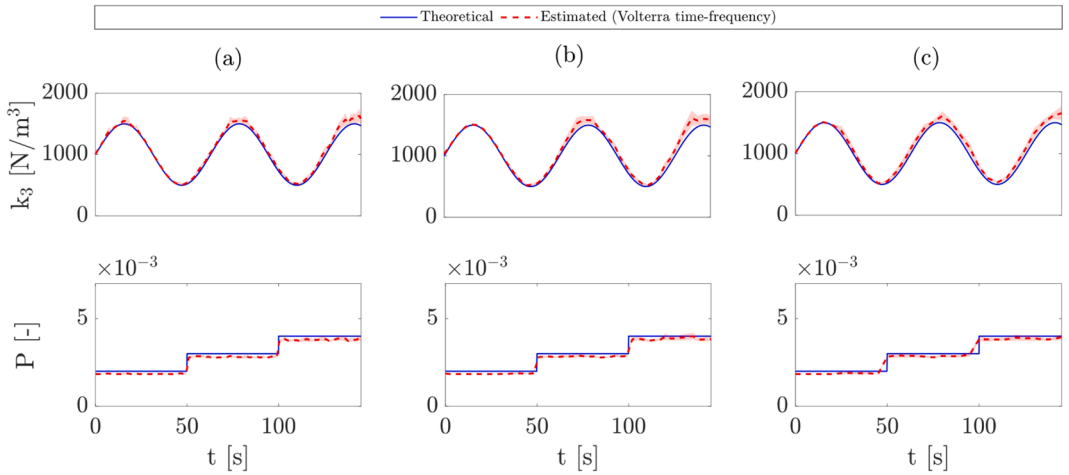


Fig. 12. Joint input-parameter estimation for $m = 5$ in case of time-varying k_3 and P: (a) WL = $15T_0$, (b) WL = $30T_0$, and (c) WL = $50T_0$.

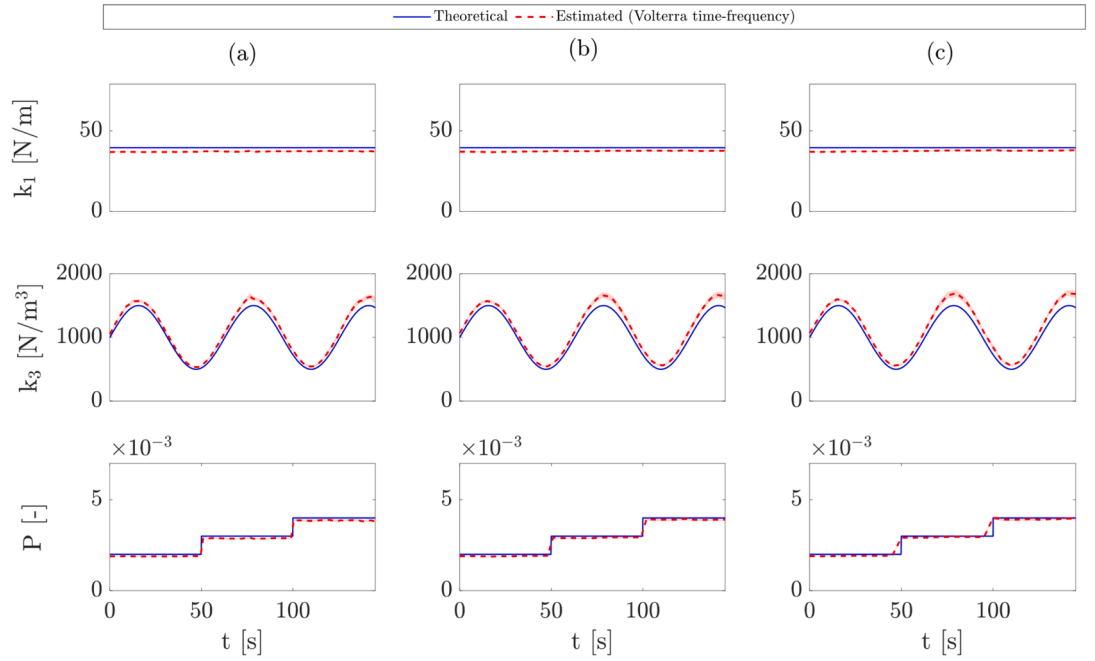


Fig. 13. Linear and non-linear parameter estimation for $m = 3$ in case of time-varying k_3 and P: (a) WL = $15T_0$, (b) WL = $30T_0$, and (c) WL = $50T_0$.

Table 2
Parameter values for the 2-DoF Duffing oscillator.

m_i [kg]	k_1 [N/m]	k_2 [N/m^2]	k_3 [N/m^3]	c [Ns/m]	P [−]
1.00	39.48	100.00	1000.00	0.38	$\{0.002, 0.003, 0.004\}$

where y_1 and y_2 are the displacements of the two masses, while u_1 and u_2 are the external inputs applied on the two masses with constant PSD $S_{u_1u_1} = S_{u_2u_2} = P/2$. The values of the parameters of the Duffing oscillator are reported in Table 2. The convergence of the Volterra series has been verified for these parameter values following the procedure outlined in [29].

A modal decomposition of the underlying linear system around the zero position reveals two vibration modes. The first mode, $\Phi_1 = \{1, 1\}^{\mathrm{T}}$, corresponding to in-phase motion of the masses, remains essentially linear, while the second mode, $\Phi_2 = \{1, -1\}^{\mathrm{T}}$, representing out-of-phase motion, carries the non-linear contributions. This is clear when transforming the system into modal coordinates q_1 and

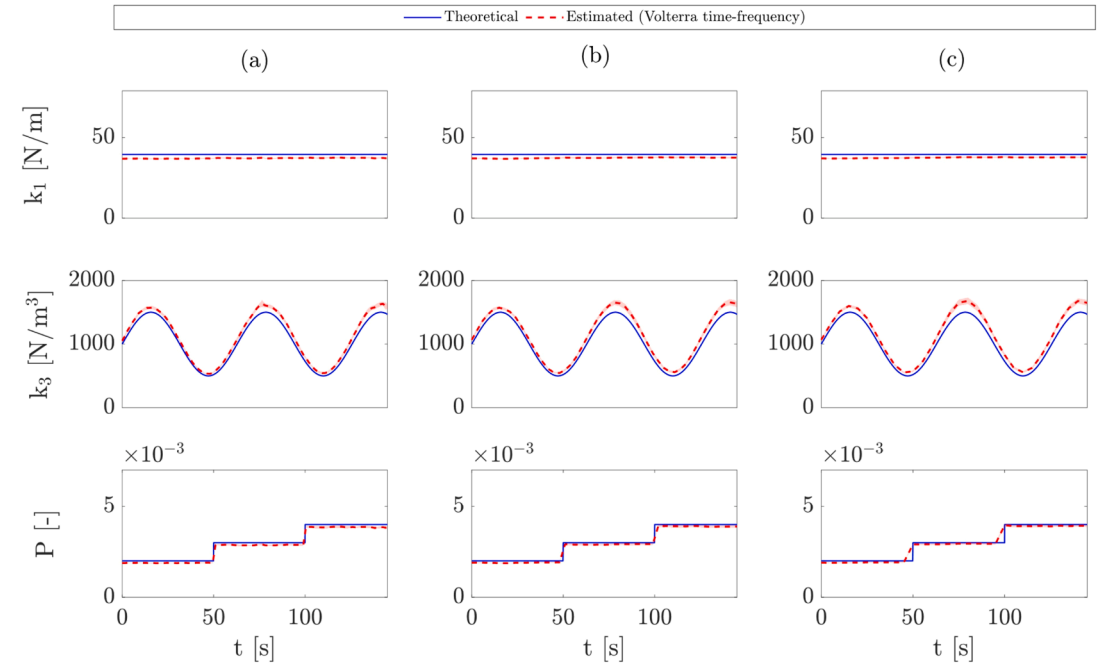


Fig. 14. Linear and non-linear parameter estimation for $m = 5$ in case of time-varying k_3 and P: (a) WL = $15T_0$, (b) WL = $30T_0$, and (c) WL = $50T_0$.

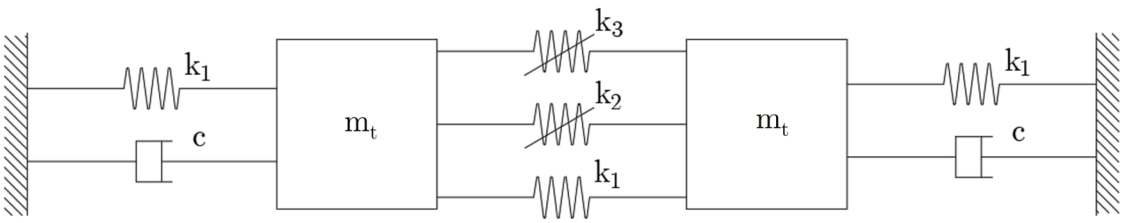


Fig. 15. Representation of the 2-DoF system.

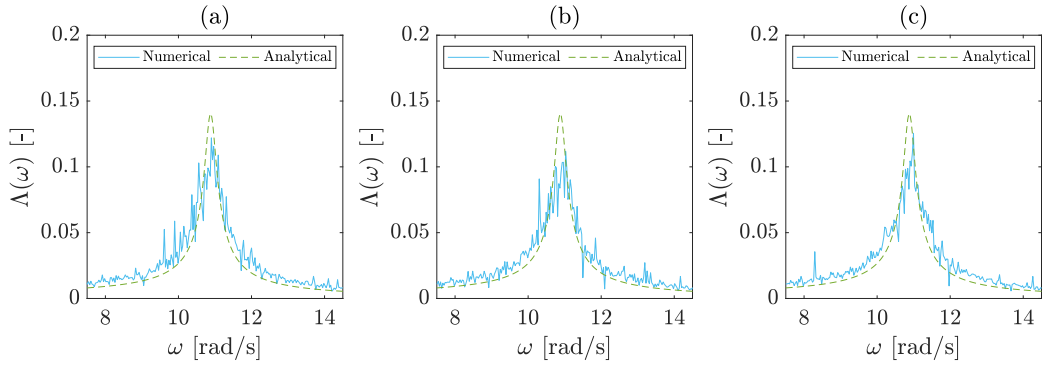


Fig. 16. Composite FRF for (a) $P = 0.002$, (b) $P = 0.003$, and (c) $P = 0.004$.

q_2:

$$\begin{cases} m_t\ddot{q}_1 + c\dot{q}_1 + k_1 q_1 = \frac{1}{\sqrt{2}}(u_1(t) + u_2(t)) \\ m_t\ddot{q}_2 + c\dot{q}_2 + 3k_1 q_2 + 2\sqrt{2}k_2 q_2^2 + 4k_3 q_2^3 = \frac{1}{\sqrt{2}}(u_1(t) - u_2(t)) \end{cases} \tag{40}$$

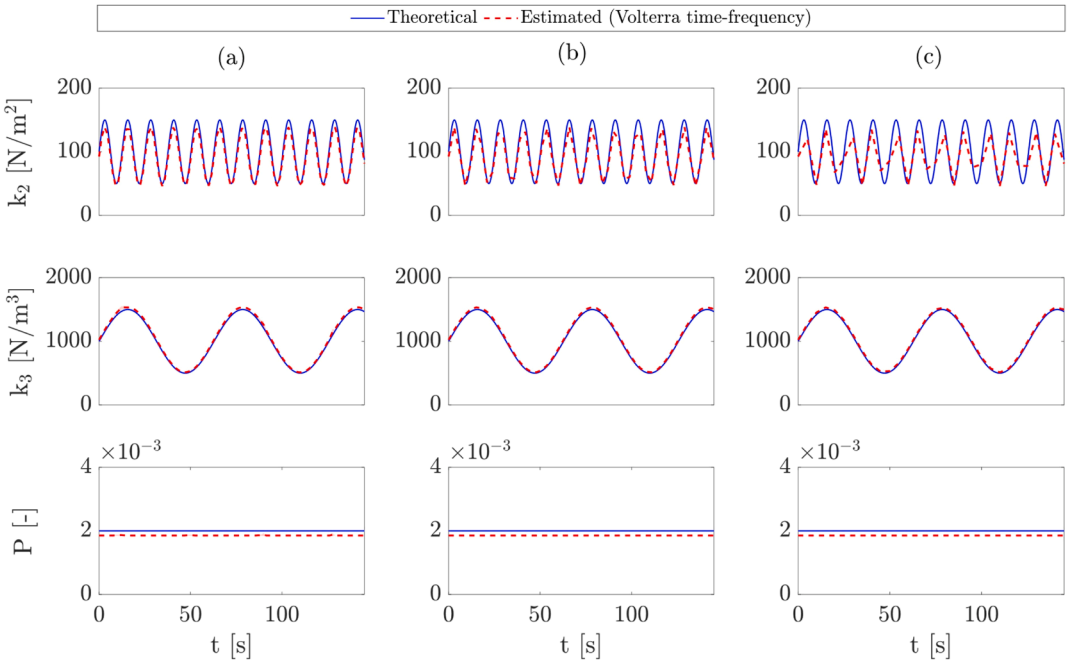


Fig. 17. Joint input-parameter estimation in case of time-varying k_2 and k_3: (a) $m = 3$ and WL $= 15T_0$, (b) $m = 3$ and WL $= 30T_0$, (c) $m = 3$ and WL $= 50T_0$.

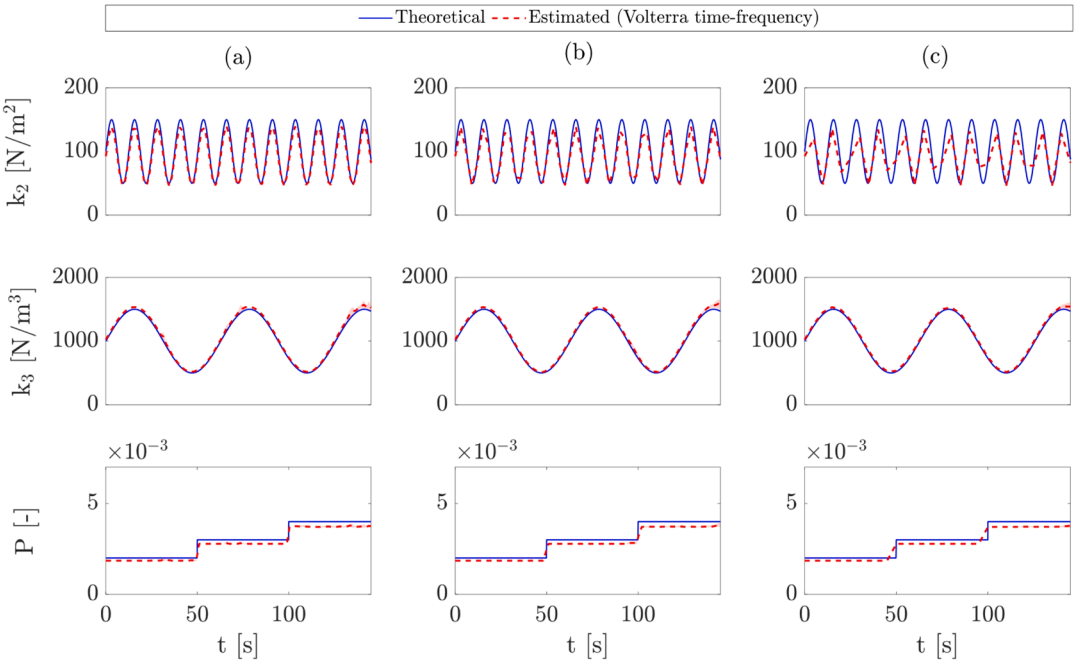


Fig. 18. Joint input-parameter estimation in case of time-varying k_2, k_3 and P: (a) $m = 3$ and WL $= 15T_0$, (b) $m = 3$ and WL $= 30T_0$, (c) $m = 3$ and WL $= 50T_0$.

with:

$$\begin{bmatrix} y_1 \\ y_2 \end{bmatrix} = \frac{1}{\sqrt{2}} \begin{bmatrix} 1 & 1 \\ 1 & -1 \end{bmatrix} \begin{bmatrix} q_1 \\ q_2 \end{bmatrix} \tag{41}$$

Importantly, from Eq. (40) it is clear that the system is decoupled into two equivalent 1-DoF systems. This property can be exploited for the purpose of non-linear parameter estimation. The FRF associated with the non-linear mode can then be used within the proposed framework to extract the non-linear and input parameters. In particular, in this case, where a quadratic non-linearity is added to the cubic one, the composite FRF associated with the modal coordinate q_2 reads:

$$\Lambda(\omega) = \frac{S_{q_2 u}(\omega)}{S_{uu}(\omega)} = H^{(1)}(\omega) + \frac{P k_2^2 H^{(1)}(\omega)^2}{c k_1^2} - \frac{3 P k_3 H^{(1)}(\omega)^2}{2 c k_1} - \frac{2 P k_2^2 H^{(1)}(\omega)^2 (\omega - 4\mathrm{i}\zeta\omega_{n,2})}{m_t c k_1 (\omega - 2\mathrm{i}\zeta\omega_{n,2})(\omega + 2\omega_{d,2} - 2\mathrm{i}\zeta\omega_{n,2})(\omega - 2\omega_{d,2} - 2\mathrm{i}\zeta\omega_{n,2})} \tag{42}$$

where $w_{n,2}$ and $w_{d,2}$ are the undamped and damped frequencies, respectively, corresponding to the second mode of vibration, and $H^{(1)}(\omega)$ can be easily deduced from the harmonic probing of the equivalent second mode 1-DoF system [29]. For this case, a Volterra series truncation order $m = 3$ was utilised.

6.1. Joint-input parameter estimation under laboratory testing conditions

The estimation task addressed in this Section considers the following parameter vector $\mathbf{p} = \{k_2, k_3, P\}$, with the cubic stiffness k_3 and input variance P defined according to Eqs. (37) and (38), and the quadratic stiffness k_2 defined as:

$$k_2(t) = 100 + 50 \sin(0.5t) \tag{43}$$

By comparing the composite FRF of Eq. (42) with the one obtained from the modal coordinate q_2, one can observe a good correspondence. This comparison, depicted in Fig. 16, proves the validity of the analytical formulation of Eq. (42).

Here, the simulation includes a 50 Hz disturbance to reproduce the mains hum [52] typical of laboratory measurements, which is one of the main sources of contamination in acquisition systems. The SNR is set to 10. The controlled injection of this noise allows the robustness of the analysis and filtering procedures to be evaluated under realistic conditions. Figs. 17 and 18 illustrate the results of joint input-parameter estimation for the system of Fig. 15 in the case of time-invariant and time-varying input variance P. The lines correspond to average values while shaded regions represents the 95% confidence bounds for the estimates obtained from 20 realisations.

The comparison between the time-invariant and time-varying parameter P case shows that, in both cases, the estimate shows fairly good agreement with theoretical values for $k_2(t)$, $k_3(t)$, and $P(t)$. Therefore, even under realistic conditions, including the presence of mains hum, the estimates are fairly accurate and the bias is low. It is important to note that the estimate of k_2 deteriorates as the length of the analysis window increases, probably due to the rapidity of the parameter variations with respect to the time window adopted.

7. Conclusions

This study set out to develop a methodology for the estimation of the instantaneous value of the parameters of time-varying non-linear dynamical systems admitting a Volterra representation. The estimation is performed in the time-frequency domain. The instantaneous PSD of the response of the dynamical system is obtained from a parametric model using Volterra theory, and it is corrected numerically to account for the distortion induced by the window function associated with the time-frequency estimator. The methodology is benchmarked for a Duffing oscillator subjected to time-varying loading and stiffness. An additional numerical example involving a 2-DoF system was also considered, simulating a laboratory-scale scenario with realistic disturbances. The estimation is conducted for different WL and SNR levels. The results reveal that the estimator is robust to noise in response signals and that bias of parameter estimates is small provided that the Volterra series convergence is satisfied.

CRediT authorship contribution statement

Linda Scussolini: Writing – original draft, Visualization, Validation, Software, Methodology, Investigation, Formal analysis, Data curation, Conceptualization; **Giuseppe Abbiati:** Writing – review & editing, Visualization, Validation, Supervision, Software, Methodology, Investigation, Data curation, Conceptualization; **Rosario Ceravolo:** Writing – review & editing, Visualization, Validation, Supervision, Resources, Project administration, Methodology, Investigation, Data curation, Conceptualization.

Funding

This research did not receive any specific grant from funding agencies in the public, commercial, or not-for-profit sectors.

Declaration of competing interest

The authors declare that they have no known competing financial interests or personal relationships that could have influenced the work reported in this paper.

Data availability

Data will be made available on request.

References

[1] G. Kerschen, K. Worden, A.F. Vakakis, J.-C. Golinval, Past, present and future of nonlinear system identification in structural dynamics, Mech. Syst. Signal Process. 20 (3) (2006) 505–592. https://doi.org/10.1016/j.ymssp.2005.04.008

[2] M.B. Priestley, Power spectral analysis of non-stationary random processes, J. Sound Vib. 6 (1) (1967) 86–97. https://doi.org/10.1016/0022-460X(67)90160-5

[3] J.N. Yang, S. Lin, On-line identification of non-linear hysteretic structures using an adaptive tracking technique, Int. J. Non-Linear Mech. 39 (9) (2004) 1481–1491. https://doi.org/10.1016/j.ijnonlinmec.2004.02.010

[4] J.N. Yang, S. Lin, H. Huang, L. Zhou, An adaptive extended Kalman filter for structural damage identification, Struct. Control Health Monit.: Off. J. Int. Assoc. Struct. Control Monit. Eur. Assoc. Control Struct. 13 (4) (2006) 849–867. https://doi.org/10.1002/stc.84

[5] M. Wu, A. Smyth, Real-time parameter estimation for degrading and pinching hysteretic models, Int. J. Non-Linear Mech. 43 (9) (2008) 822–833. https://doi.org/10.1016/j.ijnonlinmec.2008.05.010

[6] L. Cohen, Time-Frequency Analysis, Vol. 778, Prentice Hall PTR New Jersey, 1995.

[7] R. Ceravolo, Time–frequency analysis, Encycl. Struct. Health Monit. (2009). https://doi.org/10.1002/9780470061626.shm047

[8] P.J. Loughlin, L. Cohen, The uncertainty principle: global, local, or both?, IEEE Trans. Signal Process. 52 (5) (2004) 1218–1227. https://doi.org/10.1109/TSP.2004.826160

[9] R. Carmona, W.-L. Hwang, B. Torresani, Practical Time-Frequency Analysis: Gabor and Wavelet Transforms, with an Implementation in S, Academic Press, 1998.

[10] F. Auger, É. Chassande-Mottin, Quadratic time-frequency analysis I: Cohen's class, Time-Freq. Anal.: Concepts Methods (2008) 131–163. https://doi.org/10.1002/9780470611203.CH5

[11] L. Debnath, F. Shah, The Wigner-Ville distribution and time-frequency signal analysis, Wavelet Transforms Their Appl. (2002) 307–360. https://doi.org/10.1007/978-0-8176-8418-1_5

[12] L.J. Stankovic, S. Stankovic, An analysis of instantaneous frequency representation using time-frequency distributions-generalized Wigner distribution, IEEE Trans. Signal Process. 43 (2) (1995) 549–552. https://doi.org/10.1109/78.348139

[13] G. Palm, T. Poggio, The Volterra representation and the Wiener expansion: validity and pitfalls, SIAM J. Appl. Math. 33 (2) (1977) 195–216. https://doi.org/10.1137/0133012

[14] M. Schetzen, The Volterra and Wiener Theories of Nonlinear Systems, Krieger Publishing Co., Inc., 2006.

[15] S.A. Billings, Nonlinear System Identification: NARMAX Methods in the Time, Frequency, and Spatio-Temporal Domains, John Wiley & Sons, 2013. https://doi.org/10.1002/9781118535561

[16] L.J. Tick, The estimation of "transfer functions" of quadratic systems, Technometrics 3 (4) (1961) 563–567. https://doi.org/10.2307/1266562

[17] D.R. Brillinger, The identification of polynomial systems by means of higher order spectra, J. Sound Vib. 12 (3) (1970) 301–313. https://doi.org/10.1016/0022-460X(70)90074-X

[18] Y.W. Lee, M. Schetzen, Measurement of the Wiener kernels of a non-linear system by cross-correlation, Int. J. Control 2 (3) (1965) 237–254. https://doi.org/10.1080/00207176508905543

[19] R.J. Simpson, H.M. Power, Correlation techniques for the identification of non-linear systems, Meas. Control 5 (8) (1972) 316–321. https://doi.org/10.1177/002029407200500802

[20] S.A. Billings, S.Y. Fakhouri, Identification of a class of nonlinear systems using correlation analysis, in: Proceedings of the Institution of Electrical Engineers, vol. 125, IET, 1978, pp. 691–697. https://doi.org/10.1049/piee.1978.0161

[21] S. Klein, S. Yasui, Nonlinear systems analysis with non-Gaussian white stimuli; general basis functionals and kernels (Corresp.), IEEE Trans. Inf. Theory 25 (4) (1979) 495–500. https://doi.org/10.1109/TIT.1979.1056054

[22] Y. Goussard, W. Krenz, L. Stark, An improvement of the Lee and Schetzen cross-correlation method, IEEE Trans. Autom. Control 30 (9) (1985) 895–898. https://doi.org/10.1109/TAC.1985.1104086

[23] K.I. Kim, E.J. Powers, A digital method of modeling quadratically nonlinear systems with a general random input, IEEE Trans. Acoust. Speech Signal Process. 36 (11) (1988) 1758–1769. https://doi.org/10.1109/29.9013

[24] S.A. Billings, K.M. Tsang, Spectral analysis for non-linear systems, Part I: parametric non-linear spectral analysis, Mech. Syst. Signal Process. 3 (4) (1989) 319–339. https://doi.org/10.1016/0888-3270(89)90041-1

[25] S.A. Billings, K.M. Tsang, Spectral analysis for non-linear systems, Part II: interpretation of non-linear frequency response functions, Mech. Syst. Signal Process. 3 (4) (1989) 341–359. https://doi.org/10.1016/0888-3270(89)90042-3

[26] A. Chatterjee, N.S. Vyas, Non-linear parameter estimation with Volterra series using the method of recursive iteration through harmonic probing, J. Sound Vib. 268 (4) (2003) 657–678. https://doi.org/10.1016/S0022-460X(02)01537-7

[27] P. Koukoulas, N. Kalouptsidis, Third order Volterra system identification, in: 1997 IEEE International Conference on Acoustics, Speech, and Signal Processing, vol. 3, IEEE, 1997, pp. 2405–2408. https://doi.org/10.1109/ICASSP.1997.599540

[28] P. Koukoulas, N. Kalouptsidis, Second-order Volterra system identification, IEEE Trans. Signal Process. 48 (12) (2000) 3574–3577. https://doi.org/10.1109/78.887051

[29] K. Worden, Nonlinearity in Structural Dynamics: Detection, Identification and Modelling, CRC Press, 2019. https://doi.org/10.1201/9780429138331

[30] J.E. Chance, K. Worden, G.R. Tomlinson, Frequency domain analysis of NARX neural networks, J. Sound Vib. 213 (5) (1998) 915–941. https://doi.org/10.1006/jsvi.1998.1539

[31] K. Worden, G. Manson, G.R. Tomlinson, A harmonic probing algorithm for the multi-input Volterra series, J. Sound Vib. 201 (1) (1997) 67–84. https://doi.org/10.1006/jsvi.1996.0746

[32] K. Worden, G. Manson, E.J. Cross, On Gaussian process NARX models and their higher-order frequency response functions, in: Solving Computationally Expensive Engineering Problems: Methods and Applications, Springer, 2014, pp. 315–335. https://doi.org/10.1007/978-3-319-08985-0_14

[33] R. Ruotolo, C. Surace, P. Crespo, D. Storer, Harmonic analysis of the vibrations of a cantilevered beam with a closing crack, Comput. Struct. 61 (6) (1996) 1057–1074. https://doi.org/10.1016/0045-7949(96)00184-8

[34] W. Luo, S.A. Billings, Adaptive model selection and estimation for nonlinear systems using a sliding data window, Signal Process. 46 (2) (1995) 179–202. https://doi.org/10.1016/0165-1684(95)00081-N

[35] B. Weng, K.E. Barner, Time-varying Volterra system identification using Kalman filtering, in: 2006 40th Annual Conference on Information Sciences and Systems, IEEE, 2006, pp. 1617–1622. https://doi.org/10.1109/CISS.2006.286394

[36] L.G.G. Villani, S. da Silva, A. Cunha, Jr, An optimizationless stochastic volterra series approach for nonlinear model identification, J. Braz. Soc. Mech. Sci. Eng. 44 (6) (2022) 260. https://doi.org/10.1007/s40430-022-03558-z

[37] G.V. Demarie, R. Ceravolo, D. Sabia, P. Argoul, Experimental identification of beams with localized nonlinearities, J. Vib. Control 17 (11) (2011) 1721–1732. https://doi.org/10.1177/1077546310385287

[38] R. Ceravolo, G.V. Demarie, S. Erlicher, Instantaneous identification of degrading hysteretic oscillators under earthquake excitation, Struct. Health Monit. 9 (5) (2010) 447–464. https://doi.org/10.1177/1475921710368202

[39] G.D. Gkikas, Development of a novel time-frequency enhanced Volterra system identification method for the modeling of a nonlinear OWC wave energy converter under irregular sea wave excitation, in: International Conference on Offshore Mechanics and Arctic Engineering, vol. 45509, American Society of Mechanical Engineers, 2014, p. V08AT06A039. https://doi.org/10.1115/OMAE2014-23436

[40] K. Worden, G. Manson, Random vibrations of a Duffing oscillator using the Volterra series, J. Sound Vib. 4 (217) (1998) 781–789. https://doi.org/10.1006/JSVI.1998.1813
[41] S.A. Billings, H. Zhang, Computation of non-linear transfer functions when constant terms are present, Mech. Syst. Signal Process. 9 (5) (1995) 537–553. https://doi.org/10.1006/mssp.1995.0041
[42] Y. Wang, Time–frequency domain local spectral analysis of seismic signals with multiple windows, Proc. R. Soc. A 478 (2265) (2022) 20220251. https://doi.org/10.1098/rspa.2022.0251
[43] L. Cohen, Time-frequency distributions-a review, Proc. IEEE 77 (7) (1989) 941–981. https://doi.org/10.1109/5.30749
[44] J.S. Bendat, A.G. Piersol, Random Data: Analysis and Measurement Procedures, Wiley series in probability and statistics, Wiley, Hoboken, N.J, 4th ed., 2010. https://doi.org/10.1002/9781118032428
[45] X.-J. Dong, Z.-K. Peng, W.-M. Zhang, G. Meng, F.-L. Chu, Parametric characteristic of the random vibration response of nonlinear systems, Acta Mech. Sin. 29 (2) (2013) 267–283. https://doi.org/10.1007/s10409-013-0019-0
[46] P. Marzocca, J.M. Nichols, A. Milanese, M. Seaver, S.T. Trickey, Second-order spectra for quadratic nonlinear systems by Volterra functional series: analytical description and numerical simulation, Mech. Syst. Signal Process. 22 (8) (2008) 1882–1895. https://doi.org/10.1016/j.ymssp.2008.02.002
[47] G. Czanner, S.V. Sarma, U.T. Eden, E.N. Brown, A signal-to-noise ratio estimator for generalized linear model systems, in: Proceedings of the World Congress on Engineering, vol. 2, Citeseer, 2008, pp. 1063–1069.
[48] D. Simon, Optimal State Estimation: Kalman, H_∞, and Nonlinear Approaches, John Wiley & Sons, Inc., Hoboken, NJ, USA, 2006. https://doi.org/10.1002/0470045345
[49] Y. Zhang, Y. Ding, J. Bu, L. Guo, A novel adaptive square root UKF with forgetting factor for the time-variant parameter identification, Struct. Control Health Monit. 2023 (1) (2023) 4160146. https://doi.org/10.1155/2023/4160146
[50] S.S. Bisht, M.P. Singh, An adaptive unscented Kalman filter for tracking sudden stiffness changes, Mech. Syst. Signal Process. 49 (1-2) (2014) 181–195. https://doi.org/10.1016/J.YMSSP.2014.04.009
[51] M.R. Hernandez-Garcia, S.F. Masri, R. Ghanem, E. Figueiredo, C.R. Farrar, An experimental investigation of change detection in uncertain chain-like systems, J. Sound Vib. 329 (12) (2010) 2395–2409. https://doi.org/10.1016/j.jsv.2009.12.024
[52] R.W. Knapp, N.L. Anderson, Digital hum filtering, Comput. Geosci. 20 (5) (1994) 881–888. https://doi.org/10.1016/0098-3004(94)90119-8